JCI insight

RESEARCH ARTICLE

Cholesterol 25-hydroxylase promotes efferocytosis and resolution of lung inflammation

Jennifer H. Madenspacher,[1] Eric D. Morrell,[2] Kymberly M. Gowdy,[3,4] Jeffrey G. McDonald,[5] Bonne M. Thompson,[5] Ginger Muse,[1] Jennifer Martinez,[1] Seddon Thomas,[1] Carmen Mikacenic,[2] Jerry A. Nick,[6] Edward Abraham,[7] Stavros Garantziotis,[1] Renee D. Stapleton,[8] Julie M. Meacham,[1] Mary Jane Thomassen,[9] William J. Janssen,[6] Donald N. Cook,[1] Mark M. Wurfel,[2] and Michael B. Fessler[1]

[1]Immunity, Inflammation and Disease Laboratory, National Institute of Environmental Health Sciences (NIEHS), NIH, Research Triangle Park, North Carolina, USA. [2]Section of Pulmonary, Critical Care, and Sleep Medicine, Harborview Medical Center, Seattle, Washington, USA. [3]Division of Pulmonary, Critical Care and Sleep Medicine, and [4]Davis Heart and Lung Research Institute, The Ohio State University Wexner Medical Center, Columbus, Ohio, USA. [5]Department of Molecular Genetics, University of Texas Southwestern Medical Center, Dallas, Texas, USA. [6]Department of Medicine, National Jewish Health, Denver, Colorado, USA. [7]Department of Medicine, Leonard M. Miller School of Medicine, University of Miami, Miami, Florida, USA. [8]Department of Medicine, Larner College of Medicine, University of Vermont, Burlington, Vermont, USA. [9]Department of Internal Medicine, Brody School of Medicine, East Carolina University, Greenville, North Carolina, USA.

Alveolar macrophages (AM) play a central role in initiation and resolution of lung inflammation, but the integration of these opposing core functions is poorly understood. AM expression of cholesterol 25-hydroxylase (CH25H), the primary biosynthetic enzyme for 25-hydroxycholesterol (25HC), far exceeds the expression of macrophages in other tissues, but no role for CH25H has been defined in lung biology. As 25HC is an agonist for the antiinflammatory nuclear receptor, liver X receptor (LXR), we speculated that CH25H might regulate inflammatory homeostasis in the lung. Here, we show that, of natural oxysterols or sterols, 25HC is induced in the inflamed lung of mice and humans. *Ch25h*$^{-/-}$ mice fail to induce 25HC and LXR target genes in the lung after LPS inhalation and exhibit delayed resolution of airway neutrophilia, which can be rescued by systemic treatment with either 25HC or synthetic LXR agonists. LXR-null mice also display delayed resolution, suggesting that native oxysterols promote resolution. During resolution, *Ch25h* is induced in macrophages upon their encounter with apoptotic cells and is required for LXR-dependent prevention of AM lipid overload, induction of *Mertk*, efferocytic resolution of airway neutrophilia, and induction of TGF-β. CH25H/25HC/LXR is, thus, an inducible metabolic axis that programs AMs for efferocytic resolution of inflammation.

Introduction

Tissue-resident macrophages orchestrate initiation and resolution of inflammation. In response to environmental challenges such as LPS, macrophages generate temporal waves of mediators that recruit polymorphonuclear leukocytes (PMNs) and then monocytes from the circulation. The latter differentiate after arrival into macrophages with distinct transcriptional and metabolic profiles from their tissue-resident counterparts (1). Resident and recruited macrophages, instructed by an evolving cocktail of signals in the local inflammatory milieu, then drive resolution through phagocytic clearance of apoptotic cells (ACs) (i.e., efferocytosis) (2, 3). Binding and internalization of ACs engages antiinflammatory programs in macrophages (4, 5) and also feeds forward to sustain efferocytosis through activation of liver X receptor (LXR) and other transcription factors that upregulate efferocytic receptors, such as MERTK (6, 7).

In the special case of the lung, apoptotic PMNs must be quietly and efficiently cleared in order to preserve tissue integrity and vital gas exchange. However, resident alveolar macrophages (AMs) express a narrow complement of efferocytic receptors (MERTK and AXL; absent/low expression of other receptors; refs. 3, 8, 9) and

Conflict of interest: The authors have declared that no conflict of interest exists.

Submitted: February 11, 2020
Accepted: April 23, 2020
Published: June 4, 2020.

Reference information: *JCI Insight*. 2020;5(11):e137189. https://doi.org/10.1172/jci.insight.137189.

have low efferocytic function compared with macrophages in other tissues (10, 11). Although AM efferocytosis increases after LPS exposure and is thought to be primarily driven by recruited CD11c^{lo}CD11b^{hi} macrophages (1–3), few of the local signals that augment AM efferocytosis during inflammation have been identified (12). Moreover, the intracellular signals within macrophages that link AC engagement to LXR and MERTK activation remain poorly defined.

Oxysterols (i.e., oxidized species of cholesterol), have been studied for many years as feedback inhibitors of cellular cholesterol accumulation through their activation of LXR (13). Although 25-hydroxycholesterol (25HC) has, in particular, long been used in cell-based studies, mice deleted for cholesterol 25-hydroxylase (*Ch25h*), encoding the primary 25HC-synthetic enzyme, have grossly normal lipid metabolism (14). Concentrations of 25HC in human tissues are also far lower than those of other oxysterols (15). Thus, for many years, the physiologic relevance of 25HC was questioned. Recently, however, it was discovered that LPS dramatically induces *Ch25h* (>100-fold) and 25HC (>80-fold) in cultured macrophages (16–19). 25HC has now been shown to have potent anti- and proinflammatory functions in different contexts, suppressing inflammasome activation (20) and supporting M2 macrophage programming (21), but also amplifying proinflammatory cytokine induction by TLR ligands (22). Collectively, these findings have suggested that *Ch25h* is an immune-response gene induced in both inflammatory and regulatory settings, and that CH25H and its product, 25HC, may thus have context-dependent (i.e., tissue microenvironment-dependent) functions.

In mice, *Ch25h* is by far most highly expressed in the lung (23). Remarkably, AM *Ch25h* expression exceeds that of macrophages in other tissues by > 10-fold (24). This suggested to us an important role for *Ch25h* in lung inflammation. Here, we report that 25HC is the only oxysterol induced by LPS in the mouse lung and that its induction requires *Ch25h*. AM *Ch25h* is induced robustly but transiently in resident AMs early in inflammation and also in recruited AMs later, during the resolution phase of inflammation. We show that *Ch25h* is induced in resolution-phase macrophages upon their encounter with ACs and that it is required for *Mertk* induction and LXR-dependent efferocytic resolution of neutrophilia. Suggesting relevance to humans, *Ch25h* is induced by LPS in human AMs, and 25HC is induced in the airspace of LPS-exposed human volunteers. Moreover, we show that, in acute respiratory distress syndrome (ARDS) patients, AM *CH25H* expression tracks with AM *MERTK* and bronchoalveolar lavage fluid (BALF) 25HC. Taken together, we identify CH25H/25HC/LXR as a temporally inducible metabolic axis that contributes to AM reprogramming for resolution of inflammation.

Results

LPS triggers robust and selective induction of 25HC in murine and human lung. LXR is an oxysterol-activated nuclear receptor that coordinately suppresses cellular cholesterol accumulation and inflammation. Upon sensing an excess of intracellular desmosterol or oxysterols (i.e., 24[S]HC; 25HC; 27HC), LXR induces genes that encode sterol efflux transporters (e.g., ATP-binding cassette a1 *[Abc]a1*, *Abcg1*) and also transrepresses NF-κB (13). We have previously shown that treatment of mice with a synthetic LXR agonist reduces LPS-induced lung inflammation (25). Given this, we speculated that native oxysterols might also be induced in the lung following LPS and then act through autocrine or paracrine mechanisms to modulate inflammation through LXR. To this end, we exposed C57BL/6 mice to LPS aerosol and used liquid chromatography-mass spectrometry to screen BALF harvested at various time points for a wide panel of naturally occurring (oxy)sterols. Of 13 sterols measured, only 25HC was induced following LPS (Figure 1A and Supplemental Figure 1; supplemental material available online with this article; https://doi.org/10.1172/jci.insight.137189DS1). 25HC induction was remarkably robust, was completely *Ch25h* dependent, and was also observed in the serum of mice following LPS inhalation (Figure 1, A and B) and in the BALF of human volunteers 16 hours following bronchoscopic LPS instillation (Figure 1C). By contrast, 7α,25-HC, a downstream metabolite of 25HC that is inactive upon LXR but has chemoattractant activity through the receptor EBI2 (26), was undetectable (not shown).

Ch25h is very highly expressed in AMs compared with macrophages in other tissues (24). We found that *Ch25h* expression was ~35-fold higher in CD64^{+}F4/80^{+}CD11c^{hi}CD11b^{lo} resident AMs lavaged from the airspace of naive mice than in CD64^{lo}Ly6C^{hi} monocytes sorted from digests of naive lung parenchyma (Supplemental Figure 2). This suggests that signals in the alveolar space may induce *Ch25h* during AM differentiation. Naive *Ch25h*$^{-/-}$ mice had normal AM counts and airspace cytokine levels (Supplemental Figure 3), suggesting that CH25H is not itself overtly required for AM differentiation.

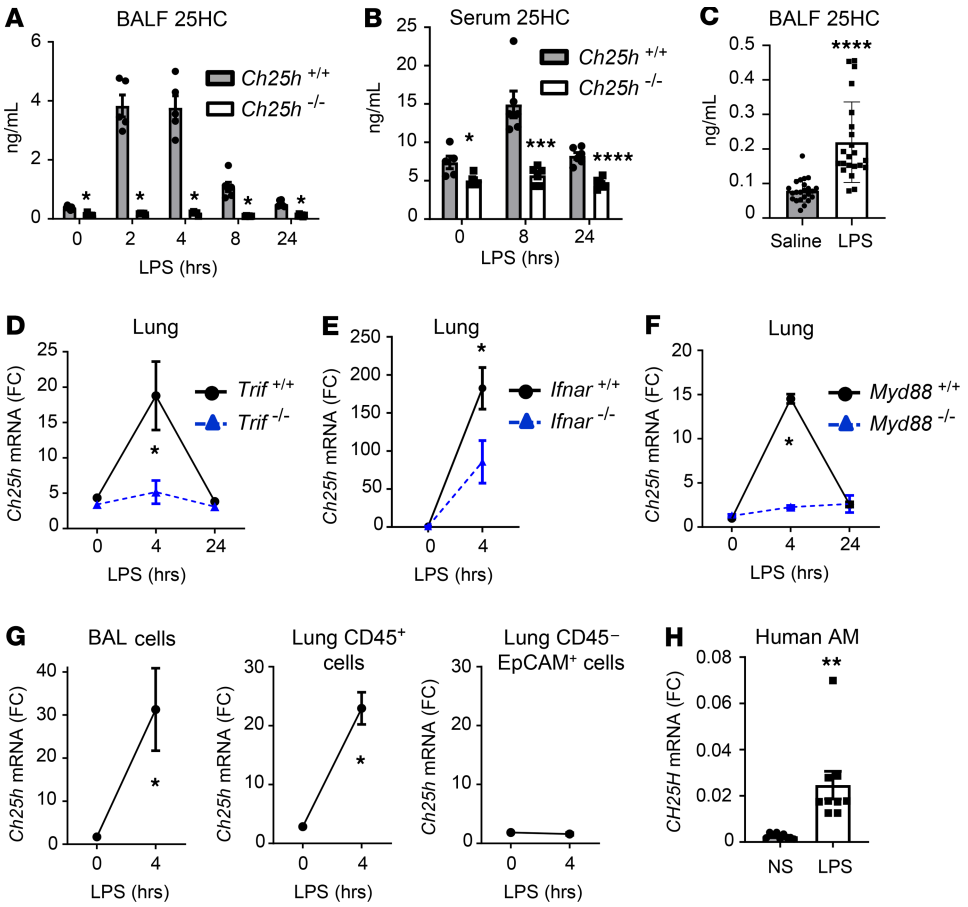

Figure 1. *Ch25h* is induced by LPS in macrophages of murine and human lung. (**A** and **B**) BALF (**A**) and serum 25HC (**B**) was quantified by liquid chromatography–mass spectrometry (LC-MS) at the indicated time points following LPS inhalation in *Ch25h*$^{+/+}$ and *Ch25h*$^{-/-}$ mice (n = 5–7/genotype/time point). (**C**) BALF 25HC was quantified 16 hours following contralateral subsegmental bronchoscopic instillation of saline and LPS into human volunteers (n = 23) (**D–F**) Lung tissue *Ch25h* mRNA (fold change [FC], normalized to *Gapdh* and indexed to WT/control) was quantified by quantitative PCR (qPCR) at various times after LPS inhalation in the murine strains indicated (n = 5/genotype/time point). (**G**) *Ch25h* mRNA (*Gapdh*-normalized) was quantified in BAL cells, and in CD45$^+$ and CD45$^-$EpCAM$^+$ cells from WT lung parenchyma at the indicated times in relation to LPS inhalation (n = 3/genotype/time point). (**H**) Alveolar macrophages (AM) collected from BAL of normal, healthy human controls (n = 3) were exposed ex vivo to LPS (10 ng/mL, 4 hours) or left nonstimulated (NS) and then assayed by qPCR for normalized *CH25H* mRNA. Data are mean ± SEM and are representative of 2–3 independent experiments. *P < 0.05; **P < 0.01; ****P < 0.0001 by unpaired t test.

Given the robust Ch25h-dependent induction of 25HC by LPS, we speculated that pulmonary *Ch25h* might be upregulated by LPS. We and others have shown that LPS induces *Ch25h* in cultured cells through a pathway involving the TLR4 adaptor TIR-domain–containing adapter–inducing IFN-β (TRIF) and downstream autocrine IFN-β signaling through its receptor, Ifnar (17, 18, 27). Consistent with this, we found that *Ch25h* was highly upregulated in WT murine lungs within 4 hours of LPS and that this was abrogated in *Trif*$^{-/-}$ mice and markedly reduced in *Ifnar*$^{-/-}$ mice (Figure 1, D and E). Pointing to an additional role for the TLR4 adaptor myeloid differentiation primary response 88 (MYD88), *Ch25h* induction was also abrogated in *Myd88*$^{-/-}$ mice (Figure 1F). Tissue fractionation studies confirmed that *Ch25h* was strongly induced by LPS in airspace leukocytes, as well as CD45$^+$ cells (leukocytes) in the lung parenchyma, but not in lung parenchymal CD45$^-$EpCAM$^+$ (epithelial) cells (Figure 1G). LPS similarly upregulated *CH25H* in primary human AMs ex vivo (Figure 1H). In a high-dose model of LPS-induced lung injury with more protracted kinetics (peak inflammation, day 3; resolution, days 6–12), we confirmed that *Ch25h* was transiently upregulated in resident (CD64$^+$F4/80$^+$CD11c^{hi}CD11b^{lo}) AMs at peak inflammation, whereas recruited AMs (CD64$^+$F4/80$^+$CD11c^{lo}CD11b^{hi}) collected by BAL downregulated *Ch25h* during early resolution, followed by a progressive recovery of expression (Supplemental Figure 4). In a cohort of 30 ARDS patients, AM *CH25H* and BALF 25HC were correlated (r = 0.47, P < 0.01), suggesting that AMs may be an important

source of 25HC in the alveolar space during clinical human lung injury (Supplemental Figure 5). Taken together, these findings indicate that *Ch25h* is a signature gene of AMs, that it is dynamically regulated in murine and human AM populations following LPS exposure, and that its product, 25HC, is unique among oxysterols in being induced and released in the inflamed lung.

Defective resolution of inflammatory neutrophilia in Ch25h-null mice. LPS inhalation triggers a self-limited inflammatory response in which cytokines/chemokines attract circulating PMNs to the airspace. In order to fully profile the effect of CH25H/25HC deficiency on induction and resolution of acute lung inflammation, we used a well-characterized low-dose LPS aerosol exposure model in which peak alveolar neutrophilia occurs by 24 hours after LPS and is then followed by clearance of PMNs by approximately 72 hours (25). Of interest, we found that *Ch25h*$^{-/-}$ mice had normal induction to peak neutrophilia but a defect in resolution of alveolar PMN counts (Figure 2A). A defect in PMN resolution was also observed following i.t. infection with the Gram-negative bacterium, *Klebsiella pneumoniae* (Figure 2B). No difference in *K. pneumoniae* burden (i.e., CFUs) was seen between *Ch25h*$^{+/+}$ and *Ch25h*$^{-/-}$ lungs 24 hours after infection (data not shown). Moreover, indicating that the deficit in resolution of neutrophilia in *Ch25h*$^{-/-}$ mice extends beyond the lung, persistent elevation of peritoneal cavity PMNs was also observed 4 days following i.p. injection with Brewer's thioglycollate (Figure 2C), a time point during which resolution is underway in this model of neutrophilic peritonitis (28).

The LPS aerosol model has well-curated kinetics, in which most cytokines and CXCR2-active (PMN-attracting) chemokines peak in the BALF by about 2 hours and then largely extinguish by about 24 hours (25, 29). Consistent with the late-phase neutrophilia in *Ch25h*$^{-/-}$ mice deriving from a deficit in PMN clearance, and not from sustained chemokine-driven influx of blood PMNs into the alveolus, we found that cytokine levels were equivalent between strains at 2 hours but that select cytokines and chemokines — including several known to attract PMNs to the airspace and/or to support their intraalveolar survival (i.e., CXCL1, CXCL5, TNF-α, IL-6, GM-CSF) — were lower in *Ch25h*$^{-/-}$ mice than WT counterparts at later time points (Figure 2, D–G). Although *Ch25h*$^{-/-}$ macrophages are reported to have derepressed inflammasome-dependent production of IL-1β (20), we observed no difference in BALF IL-1β between the 2 strains at any time point. Surface expression of CXCR2 on peripheral blood PMNs was also not substantially different between the 2 strains at 24 or 48 hours after LPS (Supplemental Figure 6). Taken together, while these findings could be consistent with 25HC induction in the airspace acting to sustain alveolar levels of select cytokines, they did not suggest that *Ch25h* deletion prolongs PMN migration into the airway and, instead, pointed to a possible deficit in clearance of PMNs.

Ch25h is required for native activation of the LXR pathway in the inflamed lung. Although LPS reportedly suppresses LXR activity in cultured macrophages (30), we nonetheless questioned whether robust induction of endogenous 25HC might support native LXR activity during inflammation in vivo. Confirming its activity as a bone fide LXR agonist, we found that, similar to the synthetic LXR agonist TO901317 (13, 25), 25HC strongly induced the LXR target genes *Abca1* and *Abcg1* in murine peritoneal exudate macrophages (PEMs) and did so in an LXR-dependent manner (Figure 3A). In vivo (i.p.) treatment of mice with 25HC also induced multiple LXR target genes, as well as the genes encoding LXRα and -β themselves (*Nr1h3* and *Nr1h2*, respectively) in the lungs of WT mice (Figures 3B). Given this, we speculated that the rapid and robust induction of native 25HC in the lungs of LPS-exposed WT but not *Ch25h*$^{-/-}$ mice might support native activation of LXR in the former strain. Indeed, consistent with this, we found that a panel of 4 LXR target genes plus *Nr1h3* and *Nr1h2* all displayed a rapid but transient induction in WT, but not *Ch25h*$^{-/-}$, lung parenchyma following LPS (Figure 3C). This gene signature suggests that the robust 25HC induction observed in the alveolus in the early hours following LPS exposure supports a wave of native LXR pathway activity in the inflamed lung. This response, however, appears to extinguish before the resolution phase of neutrophilia.

Resolution deficit in Ch25h-null mice arises from LXR pathway insufficiency. We have reported that synthetic LXR agonists reduce LPS induction of airspace cytokines in mice (25). Given that *Ch25h*$^{-/-}$ mice displayed reduced BALF cytokines after LPS, we reasoned that deficient LXR activity could not explain this phenotype and that it, instead, likely reflected an LXR-independent function of 25HC (22). On the other hand, LXR activation has also been shown to augment efferocytic clearance of PMNs (7). We thus speculated that LXR insufficiency in *Ch25h*$^{-/-}$ mice might be responsible for compromising resolution of airway neutrophilia. Consistent with this, we found that systemic treatment of *Ch25h*$^{-/-}$ but not WT mice with the selective synthetic LXR agonist GW3965 (13) reduced late-phase alveolar neutrophilia after LPS

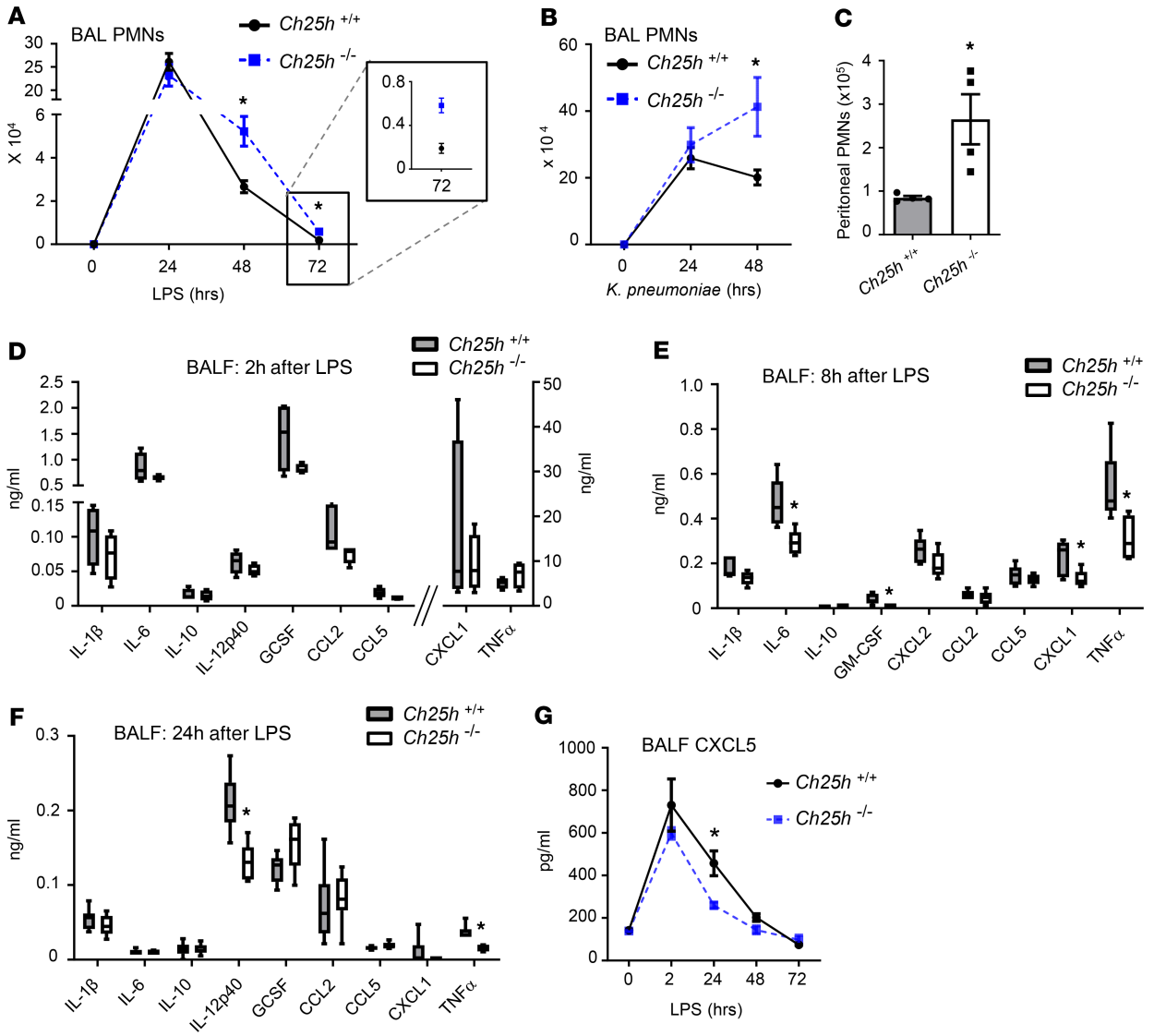

Figure 2. CH25H is required for resolution of neutrophilia. (**A** and **B**) *Ch25h*$^{+/+}$ and *Ch25h*$^{-/-}$ mice were exposed to LPS (**A**) or *K. pneumoniae* (**B**) by inhalation and then BAL polymorphonuclear neutrophils (PMNs) were quantified at the indicated times (n = 6/genotype/time point). (**C**) Peritoneal PMNs were quantified in *Ch25h*$^{+/+}$ and *Ch25h*$^{-/-}$ mice 4 days following i.p. injection of Brewer's thioglycollate (n = 4/genotype). (**D–F**) BALF was collected from *Ch25h*$^{+/+}$ and *Ch25h*$^{-/-}$ mice (n = 4–6/genotype/time point) at 2 hours (**D**), 8 hours (**E**), and 24 hours (**F**) after inhalation of LPS and analyzed for cytokine levels by multiplex assay. (**G**) BALF was collected from mice (n = 3–5/genotype/time point) at the indicated times following inhaled LPS and analyzed by ELISA for CXCL5 concentration. Data are mean ± SEM and are representative of 2–3 independent experiments. *$P < 0.05$ by unpaired t test.

(48 hours after LPS), essentially normalizing PMN counts (Figure 4A). Moreover, systemic treatment of *Ch25h*$^{-/-}$ mice with 25HC rescued late-phase alveolar neutrophilia after LPS, whereas it had no effect in LXR-deficient mice (Figure 4B), indicating that 25HC accelerates resolution via LXR. 25HC can be further processed by Cyp7b1 into 7α,25-HC (26). However, we found that *Ebi2*$^{-/-}$ mice did not phenocopy *Ch25h*$^{-/-}$ mice and, instead, exhibited a modest reduction in late-phase alveolar neutrophilia (Figure 4C). This, along with our inability to detect 7α,25-HC in the LPS-exposed lung, suggests that the failure of *Ch25h*$^{-/-}$ mice to resolve neutrophilia does not stem from 7α,25-HC deficiency.

Of interest, LXRα/β-deficient mice (Figure 4B), as well as mice singly deleted for either LXRα or LXRβ (Figure 4D), all displayed persistent late-phase alveolar neutrophilia compared with WT counterparts, supporting the notion that LXR, presumably responsive to endogenous agonists such as 25HC, is required for resolution of alveolar neutrophilia. However, LXR-deficient mice, unlike *Ch25h*$^{-/-}$ mice, also had elevated peak neutrophilia 24 hours after LPS (Figure 4D). Taken together, these findings suggest that native LXR agonists other than, or in combination with, 25HC act to repress the induction phase of

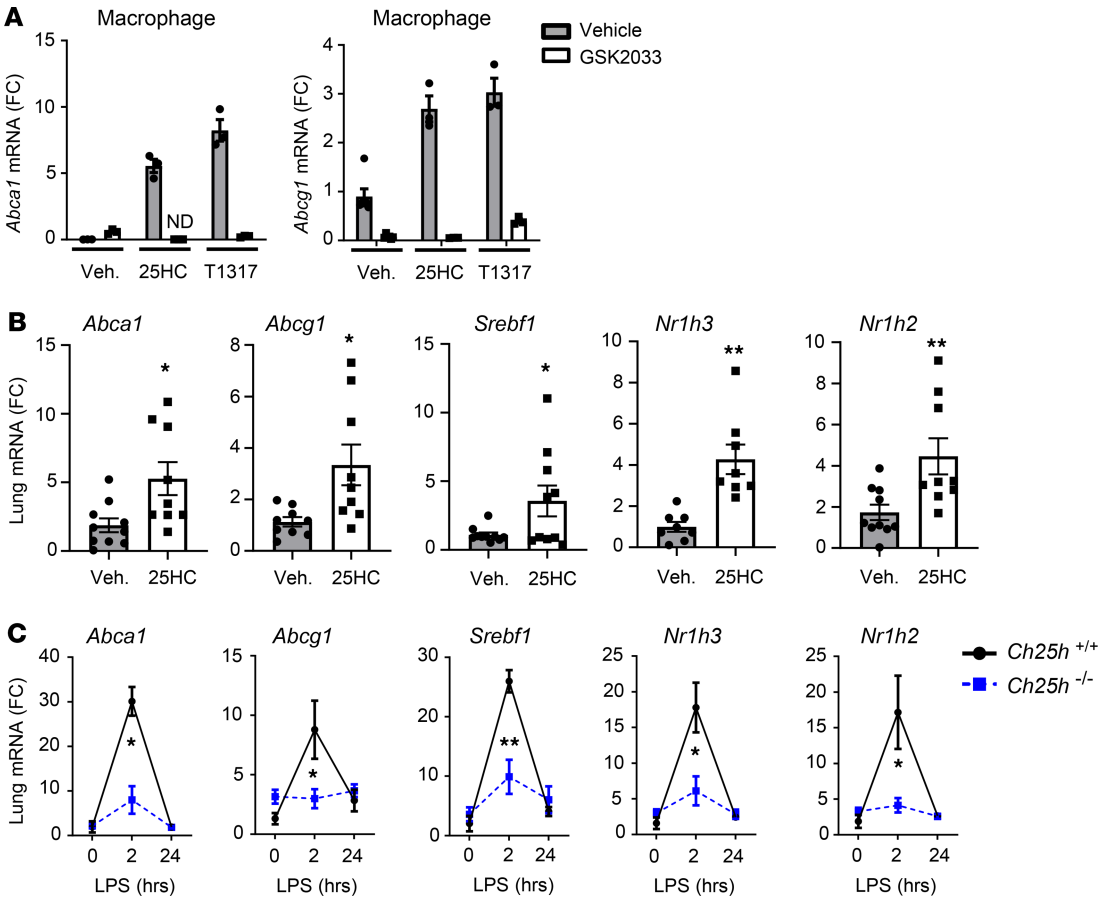

Figure 3. 25HC activates LXR in the lung. (**A**) WT peritoneal exudate macrophages (PEMs) were exposed for 16 hours to 25HC or LXR agonist TO901317 (T1317) in the presence or absence of the LXR antagonist GSK2033 and were then quantified by qPCR for *Abca1* or *Abcg1* mRNA (fold change [FC], n = 3/condition; ND, not detected). (**B**) WT mice were treated i.p. with 25HC or vehicle (Veh.), and then lung tissue was analyzed by qPCR for the targets shown (n = 8–10/condition). (**C**) *Ch25h*$^{+/+}$ and *Ch25h*$^{-/-}$ mice were exposed to inhaled LPS, and lung tissue was analyzed by qPCR for the indicated targets at the times shown (n = 4–6/genotype/time point). Data are mean ± SEM and are representative of 2–3 independent experiments. *P < 0.05; **P < 0.01 by unpaired t test.

alveolar neutrophilia, whereas 25HC deficiency is sufficient to compromise late-phase LXR-dependent clearance of PMNs from the airspace.

Ch25h deletion impairs macrophage cholesterol homeostasis and efferocytosis. Having established that the late-phase neutrophilia in *Ch25h*$^{-/-}$ mice is corrected by pharmacologic activation of LXR, and that 25HC supplementation also rescues the neutrophilia in an LXR-dependent fashion, we speculated that LXR pathway insufficiency in a pulmonary cell type was responsible for the resolution deficit. Chimeric mice generated by bone marrow transfer from WT or *Ch25h*$^{-/-}$ donors into WT or *Ch25h*$^{-/-}$ recipients revealed that *Ch25h* deletion in hematopoietic cells was sufficient to increase late-phase alveolar neutrophilia (Figure 5A). This, along with our finding that LPS robustly induces *Ch25h* in AMs (Figure 1), suggested that deficient AM 25HC might underlie the resolution failure in *Ch25h*-deficient mice.

AMs harvested from *Ch25h*$^{-/-}$ mice 48 hours after LPS had a grossly "foamy" appearance to their cytoplasm that stained positive with Oil Red O, suggesting cellular overload with neutral lipid (i.e., cholesterol) (Figure 5B). This is reminiscent of the increased macrophage foam cells reported in the lungs of mice deleted for the LXR targets *Abca1* and *Abcg1* (31, 32). Macrophages harvested from resolving peritoneal exudates similarly displayed an increased frequency of conversion to lipid-laden foam cells (Figure 5C). Suggesting that the lipid overload stemmed from LXR pathway (cholesterol efflux) insufficiency, freshly harvested PEMs from *Ch25h*$^{-/-}$ mice displayed deficient expression of a panel of LXR target genes, including *Abca1* and *Abcg1* (Figure 5D). Taken with our finding that 25HC is uniquely induced in the lung by LPS, the provocation of foam cells by *Ch25h* deletion suggests that, among native oxysterols, 25HC may be uniquely required for preventing conversion of inflammatory macrophages into foam cells. Moreover, these findings suggested to us that AM dysfunction stemming from LXR insufficiency might underlie the failure to resolve neutrophilia in *Ch25h*$^{-/-}$ mice.

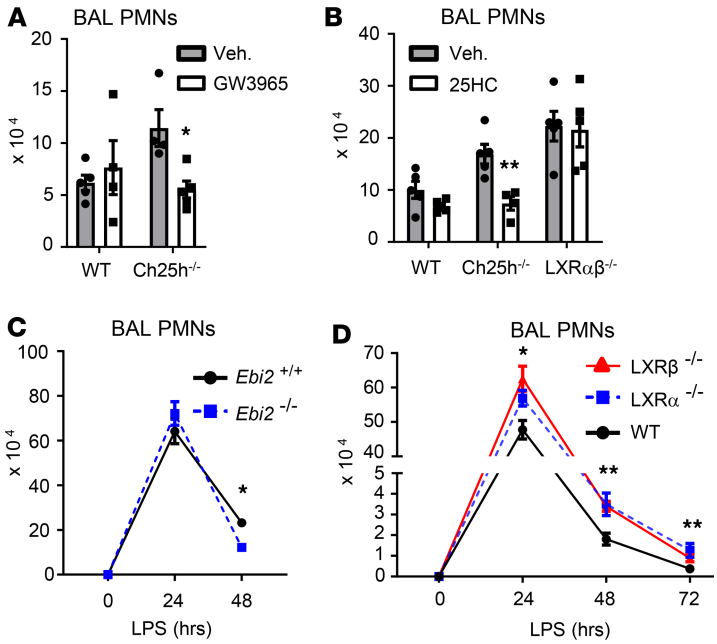

Figure 4. Defective resolution in *Ch25h*-null mice arises from LXR insufficiency. (**A** and **B**) Mice of the indicated genotypes were pretreated i.p. with either synthetic LXR agonist GW3965 (**A**) or 25HC (**B**) (or vehicle [Veh] control), exposed to inhaled LPS, and then evaluated for airway PMN count 48 hours later (n = 5/genotype/time point). (**C** and **D**) Airway PMNs were quantified in mice of the indicated genotypes at various times following inhalation of LPS (n = 5–8/genotype/time point). Data are mean ± SEM and are representative of 2–3 independent experiments. *$P < 0.05$; **$P < 0.01$ by unpaired t test.

Macrophage LXR augments efferocytic clearance of apoptotic PMNs, upregulating *Mertk* and *Abca1* (thereby effluxing cholesterol from internalized ACs) in a feedforward fashion (6, 7). Among efferocytic receptors, MERTK has been shown to play a primary role in efferocytosis by both AMs and PEMs (3, 10, 33), but the details of dynamic regulation of *Mertk* and *Abca1* by ACs — in particular, whether or not macrophage LXR is activated by sterols from internalized ACs — remain controversial (6, 34, 35). The reduced *Mertk* expression in macrophages harvested from resolving peritoneal exudates of *Ch25h*$^{-/-}$ mice (Figure 5D) suggested that their efferocytic function might be defective. Ex vivo treatment of murine macrophages with 25HC robustly induced *Mertk* in an LXR-dependent fashion (Figure 5E) and in vivo (i.p.) treatment of WT mice induced *Mertk* in lung tissue (Figure 5F), collectively supporting the notion that 25HC deficiency in *Ch25h*$^{-/-}$ mice could cause deficient pulmonary macrophage expression of *Mertk*.

In order to directly assay in vivo efferocytic function of AMs in *Ch25h*$^{-/-}$ mice during the resolution phase of inflammation, we instilled apoptotic thymocytes i.t. 48 hours after LPS; we then lavaged the airspace 90 minutes later and manually counted the frequency of AMs that had internalized ACs (36). Efferocytosis was indeed significantly decreased (mean reduction, ~41%) in AMs from *Ch25h*$^{-/-}$ mice (Figure 5G). Consistent with deficient native efferocytosis of PMNs contributing to the late-phase alveolar neutrophilia of *Ch25h*$^{-/-}$ mice, we also observed an increased frequency of uncleared apoptotic PMNs in the airspace of *Ch25h*$^{-/-}$ mice 48 hours after LPS (Figure 5H). Of interest, *Ch25h*$^{-/-}$ macrophages, by contrast, displayed normal internalization of bacterial bioparticles (Figure 5I). *Ch25h* deletion, therefore, does not globally compromise macrophage phagocytosis of all cargo. *Ch25h*$^{-/-}$ mice, as well as mice deleted for either LXRα or LXRβ, all had increased accumulation of macrophages in the alveolar space after LPS (Supplemental Figure 7), ruling out macrophage deficiency as a contributing factor to reduced efferocytic clearance of cell corpses from the airspace.

Ch25h is induced in efferocytic macrophages and required for Mertk upregulation. Aiming to better define the role of CH25H in efferocytosis, we next focused our attention directly on macrophage CH25H during efferocytic engagement of ACs. Given similar efferocytic receptor utilization in AMs and PEMs (in particular, their primary reliance on MERTK; refs. 3, 8, 33) and the relative ease of harvesting large numbers of the latter cell type, we used PEMs in our studies. Of interest, ACs (irradiated Jurkat cells; ref. 36) induced

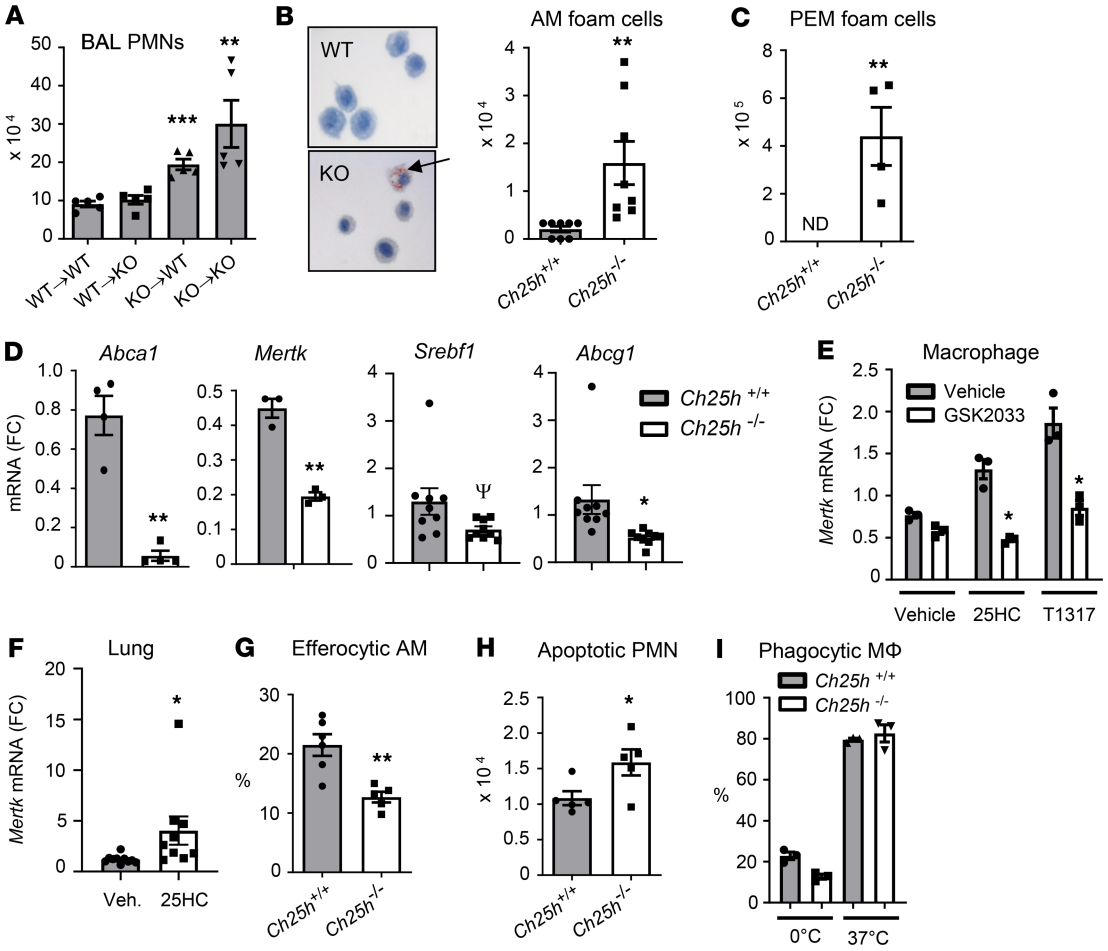

Figure 5. *Ch25h*-null macrophages display cholesterol dysregulation and defective efferocytosis. (**A**) Chimeric mice generated by bone marrow transfer from *Ch25h*$^{+/+}$ (WT) or *Ch25h*$^{-/-}$ (KO) donors to irradiated WT or KO recipients (shown as donor → recipient) were exposed to inhaled LPS, and bronchoalveolar lavage (BAL) PMNs were quantified 48 hours later (n = 5/genotype/time point). (**B**) Alveolar macrophages (AMs) from *Ch25h*$^{+/+}$ and *Ch25h*$^{-/-}$ mice collected 48 hours after LPS inhalation were stained with Oil Red O (left) and stain-positive (foam) cells quantified (right) (n = 8/genotype). Arrow indicates a stain-positive cell. (**C**) A similar analysis as shown in **B** was conducted on peritoneal exudate macrophages (PEMs) harvested 72 hours after i.p. thioglycollate (n = 4/genotype). (**D**) PEMs freshly harvested from *Ch25h*$^{+/+}$ and *Ch25h*$^{-/-}$ mice (n = 3–9/genotype) were analyzed by qPCR for the targets shown (fold change, FC). (**E**) WT PEMs were treated with 25HC or T0901317 in the presence or absence of LXR antagonist GSK2033 and then analyzed by qPCR for normalized *Mertk* mRNA. (**F**) WT mice were treated i.p. with 25HC or vehicle (Veh.), and then lung tissue was analyzed by qPCR for *Mertk* (n = 8–10/condition). (**G**) *Ch25h*$^{+/+}$ and *Ch25h*$^{-/-}$ mice (n = 6/genotype) were instilled i.t. with apoptotic WT thymocytes 48 hours after LPS inhalation. AMs that had internalized thymocytes (efferocytic AMs) were manually quantified 90 minutes later. (**H**) Apoptotic (FLIVO^{+}) PMNs were quantified in BALF of *Ch25h*$^{+/+}$ and *Ch25h*$^{-/-}$ mice (n = 5/genotype) 48 hours after LPS inhalation. (**I**) Internalization of bacterial bioparticles by *Ch25h*$^{+/+}$ and *Ch25h*$^{-/-}$ PEMs was quantified at 37°C and 0°C (control). Data are mean ± SEM and are representative of 3–6 independent experiments. $^{\Psi}$P = 0.06; *P < 0.05; **P < 0.01; ***P < 0.001 by unpaired t test.

Ch25h in WT murine macrophages (Figure 6A), indicating — together with our finding of progressive *Ch25h* induction in resolution-phase recruited AMs (Supplemental Figure 4) — that *Ch25h* is induced not only in inflammatory, but also in regulatory settings. Unlike the case for *Ch25h* induction by LPS (Figure 1), AC induction of *Ch25h* was Ifnar independent (Figure 6B).

Efferocytic receptors of the TYRO3/AXL/MERTK (TAM) family engage ACs indirectly via growth arrest specific 6 (GAS6), a secreted protein that bridges phosphatidylserine (PS) on ACs to macrophage TAMs, activating the latter (11). Treatment of macrophages with recombinant GAS6 induced sustained *Ch25h* upregulation of a similar magnitude to that induced by ACs (Figure 6C), suggesting that AC internalization may not be required for *Ch25h* induction and that *Ch25h* may instead be upregulated via signaling initiated from the cell surface. Of interest, we found that AC induction of both *Mertk* and *Abca1* was abrogated in *Ch25h*$^{-/-}$ macrophages (Figure 6D), suggesting that macrophage 25HC is required for induction of these LXR targets during efferocytosis. By contrast, induction of *Axl*, an LXR-independent TAM receptor (6), was *Ch25h* independent (Figure 6E). Compared with

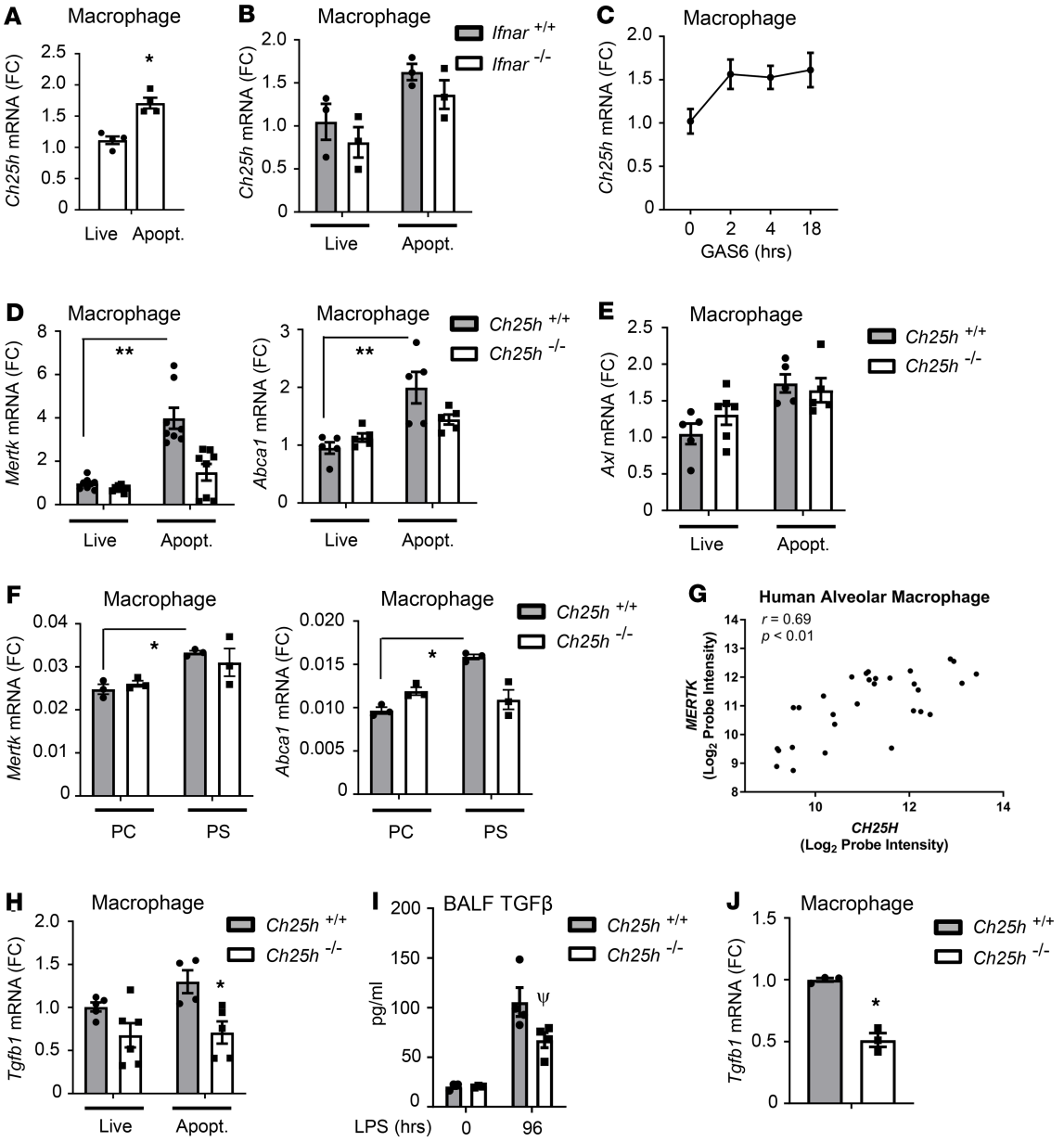

Figure 6. Apoptotic cells induce *Ch25h*-dependent *Mertk* in efferocytic macrophages. (**A**) WT peritoneal exudate macrophages (PEMs) were cocultured for 16 hours with live or apoptotic Jurkat T cells, after which *Ch25h* mRNA was quantified by qPCR (fold change [FC], $n = 4$/condition). (**B**) *Ifnar*$^{+/+}$ and *Ifnar*$^{-/-}$ PEMs were treated and analyzed as in **A** ($n = 3$/condition). (**C**) WT PEMs ($n = 4$/condition) were treated with 400 ng/mL Gas6 protein for the indicated times and then analyzed by qPCR for *Ch25h* mRNA. (**D** and **E**) *Ch25h*$^{+/+}$ and *Ch25h*$^{-/-}$ PEMs were treated as in **B** and then analyzed by qPCR for the indicated targets ($n = 5$–8/condition). (**F**) *Ch25h*$^{+/+}$ and *Ch25h*$^{-/-}$ PEMs were treated with phosphatidylserine (PS) or phosphatidylcholine (PC [control]) liposomes (400 μg/mL, 4 hours) and then analyzed by qPCR for the indicated targets ($n = 3$/condition). (**G**) RNA purified from AMs isolated by negative selection from patients ($n = 30$) enrolled within 48 hours after ARDS onset in the omega-3 fatty acids trial (50) was analyzed by microarray. A Pearson's test was used to generate a correlation coefficient between normalized $\log_2$ *CH25H* and *MERTK* probe intensities. (**H**) *Ch25h*$^{+/+}$ and *Ch25h*$^{-/-}$ PEMs were treated as in **D** and then analyzed by qPCR for *Tgfb1* mRNA ($n = 4$–6/condition). (**I**) Mice of the indicated genotypes were exposed to 3 mg/mL LPS aerosol and BALF TGF-β analyzed by ELISA ($n = 3$–4/condition). (**J**) PEMs freshly harvested from *Ch25h*$^{+/+}$ and *Ch25h*$^{-/-}$ mice were analyzed by qPCR for *Tgfb1* mRNA ($n = 3$/genotype). Data are mean ± SEM and are representative of 2–4 independent experiments. $^*P < 0.05$; $^{**}P < 0.01$; $^{\psi}P = 0.059$ by unpaired *t* test other than for **G**.

control phosphatidylcholine (PC) liposomes, AC-mimetic PS liposomes induced *Mertk* and *Abca1*, and this was also muted in *Ch25h*$^{-/-}$ macrophages (Figure 6F). This suggests that, like *Ch25h* induction, CH25H-dependent induction of LXR target genes in efferocytic macrophages does not require internalization of AC cargo. In AMs harvested from ARDS patients, we found a significant correlation between *CH25H* and *MERTK* expression ($r = 0.69$, $P < 0.01$) (Figure 6G), suggesting that native 25HC may also regulate *MERTK* expression in humans.

Efferocytosis not only guards against proinflammatory postapoptotic lysis of dead cells, but it also programs macrophages to express TGF-β and other antiinflammatory mediators (5). ACs modestly increased *Tgfb1* mRNA in WT but not *Ch25h*$^{-/-}$ macrophages (Figure 6H). While we did not detect TGF-β in BALF in our low-dose LPS aerosol model, *Ch25h*$^{-/-}$ mice had lower BALF TGF-β than WT counterparts during the resolution phase following inhalation of a high-dose (3 mg/mL) LPS aerosol (Figure 6I). We also found that macrophages freshly harvested from peritoneal exudates of *Ch25h*$^{-/-}$ mice had reduced *Tgfb1* expression (Figure 6J). Macrophage CH25H is, thus, also required to support the antiinflammatory functional consequences of efferocytosis during resolution of acute inflammation.

Discussion

Efferocytic macrophage populations and the clearance receptors they use differ across tissues, and within tissues, they differ between homeostatic and injury settings (2, 9, 37–39). Here, we identify CH25H/25HC as a metabolic axis that is induced in AMs early in inflammation, but also late in inflammation after PMN apoptosis has commenced, when it supports regulatory efferocytosis and TGF-β induction. We posit that, in both cases, *Ch25h*, encoding a lipid hydroxylase, is induced by cell signals initiated by macrophage sensing of membrane lipids — bacterial LPS and AC PS, respectively. Inflammatory versus regulatory *Ch25h* induction may, however, largely derive from distinct AM pools. Resident AMs, as sentinels of the alveolus, upregulate *Ch25h* rapidly in response to LPS and induce a transient LXR signature in lung before substantial influx of PMNs to the airspace. Consistent with reports that recruited AMs, which appear days later, are primarily responsible for efferocytosis (2), we find that, during resolution, *Ch25h* is selectively and progressively upregulated in these cells (Supplemental Figure 4). This suggests that AC-induced regulatory *Ch25h*/25HC may derive from recruited AMs, contemporaneous with the accumulation of ACs after peak PMN influx. Our findings, however, do not prove which pool of macrophage CH25H is most important to resolution, especially given that *Ch25h* expression is lower in recruited than in resident macrophages. As the contribution of CH25H to resolution of neutrophilia is partial, the physiological significance of the CH25H/25HC/LXR axis is also uncertain. Nonetheless, our rescue studies suggest potential for exogenous 25HC and synthetic LXR agonists as proresolving therapeutics, at least in low-CH25H states and perhaps other disease conditions with deficient efferocytosis.

The local factors that determine the high expression of *Ch25h* in AMs remain poorly defined. The transcription factor KLF4 is a candidate, as it has been shown to transactivate *Ch25h* in endothelial cells (40) and was recently identified as a master regulator of efferocytosis that is highly expressed by AMs (9, 41). Of interest, activating transcription factor 3, which reportedly represses *Ch25h*, is expressed at much lower levels in AMs than in pulmonary interstitial macrophages or in macrophages from several other tissues (24). Recent reports indicate that resident AMs are endowed with mechanisms to cope with local 25HC. The sterol efflux transporter ABCG1, in particular, plays a key role in mobilizing 25HC from AMs and preventing pulmonary 25HC overload (42). Neutral cholesterol ester hydrolase 1 has also been shown to protect cells from 25HC-induced ER stress (43) and is reportedly much more highly expressed in AMs than in macrophages from other tissues (44). It is, thus, intriguing to consider that AMs may be metabolically buffered against 25HC. Despite our findings using bone marrow chimeric mice, we do not exclude a possible role for endothelial CH25H. Moreover, cell-specific roles for CH25H likely differ in the human lung, where *Ch25h* expression has been reported in both AMs and pneumocytes of subjects with COPD (45).

We found that CH25H is required to prevent transformation of postinflammatory macrophages into lipid-laden foam cells. This suggests that 25HC, among oxysterols, may be uniquely required during resolution for coordinately supporting cholesterol efflux and efferocytosis through LXR. This distinguishes it from desmosterol, which accumulates in foam cells during dyslipidemia and activates LXR (46). Resolution phase 25HC may also possibly prevent cellular lipid overload by suppressing cholesterol biosynthesis (26). These protective functions of native *Ch25h*/25HC likely depend on contextual signals that are not adequately modeled by exogenous 25HC, given that treatment of bone marrow–derived macrophages and fibroblasts with 25HC reportedly promotes cytosolic lipid body accumulation (47).

Although it has been proposed that the TAM receptor AXL predominates in inflammatory settings and MERTK in regulatory settings (48), several reports have documented suppressive roles for MERTK in acute inflammation (49–51), as well as in postinflammatory efferocytosis, including in the lung (3). Despite its cleavage by proteases early in inflammation, MERTK is progressively induced (49, 52) and activated (49, 53) — likely due, at least in part, to feedforward effects of efferocytosis. Reports to date have differed on whether

(6, 7) or not (35) the sterol load of internalized ACs drives LXR-dependent induction of *Mertk* and other target genes. AC internalization may not be required for induction of ABCA1 (35) or repression of cytokines (5). Here, we show for the first time to our knowledge that macrophage *Ch25h* plays a role in efferocytosis and its transcriptional consequences. Our finding that *Ch25h* is also required for *Mertk* induction by liposomal PS suggests that AC internalization may be dispensable. Alternatively, given that *Ch25h* is itself a LXR target (54), it is also possible that *Ch25h*/25HC is required to relay and amplify primary activation of LXR by the internalized AC. Whether basal levels of 25HC are permissive for efferocytosis or whether de novo generation of 25HC is required remains unclear.

Our studies leave open the possibility of additional roles for 25HC in AC clearance. For example, 25HC reportedly activates RAC (55), a GTPase that plays a key role in efferocytosis (56). In addition, given that LPS upregulates *Ch25h* in PMNs (57), and 25HC is chemoattractive (58), it is intriguing to consider that 25HC may also possibly serve as a "find me" signal for efferocytic macrophages. 25HC also has membrane-disordering properties (59); thus, 25HC could also conceivably alter the palatability of ACs to efferocytic macrophages. Finally, it is possible that CH25H/25HC may also impact important mechanisms of resolution beyond efferocytosis, such as generation of specialized proresolving lipid mediators (e.g., resolvins) and recruitment of Tregs to the lung.

LXR-null and MERTK-null mice both reportedly develop spontaneous inflammation and autoimmune disease with age due to defective efferocytosis in their tissues (6, 60). In contrast with this, we found that neither male nor female *Ch25h*$^{-/-}$ mice aged out to 1+ years developed pathology in any of several tissues screened (e.g., kidney, lung, lymph nodes, pancreas, heart, liver, spleen, and skeletal muscle). This suggests that, while CH25H is required for postinflammatory efferocytosis, it may be dispensable for homeostatic clearance of ACs in the steady state.

In closing, we add 25HC to the list of paracrine lipids that program efferocytosis during resolution of inflammation. Future studies are warranted to better define whether the downstream effects of 25HC on inflammation and injury are dissociable and whether 25HC may be either an informative biomarker or an intervenable target in human lung disease.

Methods

Reagents. *E. coli* 0111:B4 LPS, penicillin, and streptomycin were from MilliporeSigma. *K. pneumoniae* 43816 (serotype 2), DMEM, and FBS were from American Type Culture Collection. GW3695 (MilliporeSigma), T0901317 (Cayman Chemical), 25HC (MilliporeSigma), cholesterol (MilliporeSigma), GSK2033 (MilliporeSigma), GAS6 (R&D), and PS and PC (Avanti Polar Lipids) were purchased. The Bio-Rad protein assay was used (catalog 5000006).

Mice. Female and male mice, 7–10 weeks old and weighing 18–22 g, were used. *Ch25h*$^{-/-}$ mice were produced as described (16). C57BL/6, *Myd88*$^{-/-}$, and *Ifnar*$^{-/-}$ mice were from the Jackson Laboratory. *Trif*$^{-/-}$ mice were as described (27). *Nr1h2*$^{-/-}$ and *Nr1h3*$^{-/-}$ mice were provided by David Mangelsdorf (University of Texas Southwestern Medical Center) and were intercrossed to produce *Nr1h2*$^{-/-}$ *Nr1h3*$^{-/-}$ mice. All aforementioned strains were ≥ 8 generations backcrossed to C57BL/6. In selected experiments (e.g., alveolar neutrophil counts after LPS), littermate controls were used. For other experiments, C57BL/6 controls were used. *Ebi2*$^{-/-}$ mice (i.e., B6;129S5-Gpr183^{tm1Lex}/Mmucd, identification number 032339-UCD) were obtained from the Mutant Mouse Regional Resource Center, a NIH-funded strain repository, and were donated to the MMRRC by Genentech Inc. Littermate controls were used exclusively for this strain.

In vivo murine exposures. Exposure to aerosolized LPS (300 μg/mL or 3 mg/mL, 30 minutes) was as previously described (25). *K. pneumoniae* (2000 CFU/50 μL) was delivered to lung by oropharyngeal aspiration during isoflurane anesthesia (31). In some studies, mice were treated i.p. with 50 mg/kg 25HC or vehicle (hydroxypropyl-β-cyclodextrin; Cyclo Therapeutics Inc.) at –24, –2, and +24 hours in relation to LPS exposure or sacrifice without exposure. Apoptotic thymocytes were delivered to the lungs of mice 48 hours after LPS inhalation, as previously reported (36). Briefly, thymocytes harvested from thymi of ~4-week-old C57BL/6 mice were exposed to ultraviolet radiation (312 nm) for 5 minutes, followed by culture in RPMI 1640 with 10% FBS at 37°C in 5% CO_2 for 3 hours, and were confirmed to be > 90% annexin V$^+$. Thymocytes (1×10^7 in 50 μL) were then delivered to the mouse lung by oropharyngeal aspiration during isoflurane anesthesia. At 90 minutes after thymocyte treatment, BAL was performed, and cells were centrifuged onto slides and stained using Hema-3. The efferocytic index was then manually quantified as the number of macrophages with internalized apoptotic bodies divided by the number of macrophages counted, multiplied by 100. A minimum of 200 macrophages were counted.

Human experimental studies. BAL samples from a previous study of normal healthy volunteers exposed to intrapulmonary LPS were analyzed (61). Briefly, participants were given LPS (4 ng/kg body weight; *E. coli* 0:113 LPS [NIH] in 10 mL saline) by bronchoscopic subsegmental instillation. LPS was randomized to either the lingula or right middle lobe and was immediately followed by 10 mL sterile saline deposition into a contralateral subsegment. A second bronchoscopy was performed 16 hours later, at which time both LPS- and saline-exposed subsegments underwent BAL with 150 mL saline. The BALF was then stored at –80°C until further analysis. In separate studies, normal healthy volunteers underwent BAL for collection of AMs.

Acute lung injury/ARDS patient cohort studies. BALF samples analyzed were previously collected from subjects who were enrolled at 5 North American centers for the Phase II Randomized Placebo–controlled Trial of Omega-3 Fatty Acids for the Treatment of Acute Lung Injury trial conducted from 2006–2008 (62), as previously described (63). Enrollment into the trial occurred within 48 hours of ARDS onset. All samples used for this study were obtained from subjects before they received treatment or placebo. A subset of patients had AMs purified by negative selection using antibody-labeled microbeads for CD3, CD15, CD19, CD235a, CD294, and CD326. RNA was extracted from purified AMs and hybridized to an Illumina HumanRef-8 Beadchip inclusive of 18,415 genes. Raw microarray data underwent variance stabilization and quantile normalization using the Bioconductor package *lumi* (64). The data have been deposited in the National Center for Biotechnology Information/Gene Expression Omnibus (GEO) under accession number GSE89953.

Generation of bone marrow chimeric mice. Bone marrow chimeric mice were generated as previously reported (31). Briefly, *Ch25*$^{+/+}$ mice congenic for CD45 (stock no. 002014; Jackson Laboratory) were used. Recipients were irradiated (900 rad) by a Model 431 irradiator using a ^{137}Cs source (JL Shepherd and Associates). Within 4 hours after irradiation, bone marrow (2×10^6 cells) from femurs and tibias of donor mice was injected i.v. into recipients. The efficiency of donor stem cell engraftment was determined by flow cytometry for CD45.1 (BioLegend, 110718) (*Ch25*$^{+/+}$) 9 weeks after marrow transfer on circulating myeloid cells (CD11b$^+$; BD Biosciences, 563553), B cells (CD19$^+$; BioLegend, 115520), and T cells (CD3$^+$; BD Biosciences, 553066) and at 12 weeks (death) on AMs (CD11c$^+$; eBioscience, 45-0114-82). Engraftment efficiency was greater than 94% (data not shown).

Murine BALF collection and analysis. BALF was collected immediately following sacrifice, and cells counts were performed as previously described (25). Total protein was quantified by the method of Bradford (31).

Mass spectrometric quantitation of oxysterols. Sterols and oxysterols were quantified as previously described (16). Briefly, BALF and plasma were extracted with organic solvents, and sterols and oxysterols were quantified on a 4000 QTRAP liquid chromatography mass spectrometer (Applied Biosystems) (65).

Preparation of liposomes. Liposomes composed of either 100% PC or 70% PC/30% PS were generated by lipid extrusion as previously described (66). Briefly, the lyophilized lipids were reconstituted in chloroform and then dried under a gentle stream of nitrogen gas. After this, the lipid sheets were rehydrated forming unilamellar vesicles that were extruded via sonication and multiple passages through a Hamilton syringe.

Cell harvests and culture. Mouse bone marrow–derived macrophages were prepared and cultured in DMEM containing 10% (v/v) FBS and 10% (v/v) L cell–conditioned medium as a source of M-CSF for 5 days. PEMs were harvested by peritoneal lavage 96 hours after i.p. injection of Brewer's thioglycollate (2 mL, 4% solution). PEMs were cocultured with either viable or apoptotic Jurkat cells at a 5:1 Jurkat/PEM ratio. Apoptosis was induced by UV at 60 mJ/cm^2, followed by incubation in complete media at 37°C for 2 hours. In other experiments, PEMs were treated with 400 μg/mL of either PC or PC/PS liposomes for 4 hours, after which RNA was collected for analysis.

Evaluation of foam cells. Lavage cells from the airway or peritoneum were cytospun onto a slide, stained with Oil Red O, and then manually counted for stain-positive foam cells.

Cytokine analysis. Cytokines were quantified in mice by multiplex assay (Bio-Plex, Bio-Rad) or by ELISA (CXCL5, TGF-β; R&D).

Flow cytometry and cell sorting. Lung was digested/disaggregated as previously reported (67). Anti-F4/80 (PE, 123116; APC, 123110]), -CD11c (PE-Cy5, 117316), -CXCR2 (PE-Cy5.5, 129103), -CD45 (PE, 103105), -EpCAM (APC, 118212), and isotype control antibodies (catalog 400907) were from BioLegend. Cells were stained and fixed with 2% paraformaldehyde/PBS. Flow cytometry was performed using an LSR II (BD Biosciences) and analyzed using FlowJo (Tree Star Inc.) and FCS Express (De Novo Software) software. Resident AMs (CD64$^+$F4/80$^+$CD11c^{hi}CD11b^{lo}Siglec-F^{hi}), recruited AMs (CD64$^+$F4/80$^+$CD11c^{hi}CD11b^{lo}Siglec-F^{lo}), and lung parenchymal monocytes (CD64^{lo}SSC^{lo}Ly6C^{hi}) were identified and purified by fluorescence-activated cell sorting, as previously reported (1).

RNA-Sequencing (Seq). RNA-Seq and downstream analysis was performed as previously reported (1). The data have been deposited in the National Center for Biotechnology Information/GEO under accession number GSE94749.

Assessment of apoptosis. PMNs ($Ly6G^+$; BioLegend, 127610) lavaged from the murine airway were incubated (60 minutes, 37°C) ex vivo with 1 μL (1:50 DMSO) of FLIVO, a cell-permeant fluorescent polycaspase activity reporter (Immunochemistry); they were then washed twice (0.5% BSA in 1× PBS, pH 7.4). Fluorescence signal was quantified by flow cytometry.

RNA isolation and quantitative PCR. RNA was isolated by RNEasy kit (QIAGEN). Complementary DNAs (cDNA) was generated from 1.5 μg of purified RNA using TaqMan reverse transcription reagents from Applied Biosystems. Real-time PCR was performed in triplicate with TaqMan PCR Mix (Applied Biosystems) in the HT7900 ABI sequence Detection System (Applied Biosystems). Predesigned primers were purchased from Thermo Fisher Scientific: *Nr1h2* (Mm00437265_g1); *Nr1h3* (Mm00443451_m1); *Abca1* (Mm00442646_m1); *Abcg1* (Mm00437390_m1); *Ch25h* (Mm00515486_s1); *Srebf1* (Mm00550338_m1); *Axl* (Mm00437221_m1); *Mertk* (Mm00434920_m1); *Tgfb1* (Mm01178820_m1); *Gapdh* (Mm99999915_g1), *CH25H* (Hs02379634_s1); and *GUSB* (Hs00939627_m1). Gene expression was normalized to *Gapdh* in analyses of mouse cells/tissues and normalized to *GUSB* in the studies involving ex vivo exposure of human AMs.

Histopathologic analysis. Tissues were fixed in 10% neutral-buffered formalin, trimmed, processed for paraffin, embedded, sectioned (5 μm), and stained with H&E. Slides were scanned using an Aperio ScanScope XT Scanner (Aperio Technologies Inc.). Tissues (kidney, lung, spleen, thymus, mesenteric lymph node, submandibular lymph node, heart, pancreas, liver, gall bladder, and skeletal muscle) of naive ~1-year-old $Ch25h^{+/+}$ and $Ch25h^{-/-}$ mice were evaluated for pathology by a board-certified veterinary pathologist blinded to genotype.

Statistics. For murine cell and animal studies, analyses were performed using GraphPad Prism software. Data are represented as mean ± SEM. Two-tailed Student's *t* tests were applied for comparisons of 2 groups, and 1-way ANOVA was used for comparisons of > 2 groups. For the patient studies, 25HC concentration and microarray probe intensities were analyzed as continuous variables after $\log_2$ transformation given the distribution of the data. Eighteen of the 81 BALF specimens had a 25HC concentration below the lower limit of detection (LLOD) of 0.05 ng/mL. These specimens were assigned a 25HC concentration of half the LLOD.

A Pearson's test was used to identify correlations between AM *CH25H* $\log_2$ probe intensity and AM *MERTK* $\log_2$ probe intensity, as well as AM *CH25H* $\log_2$ probe intensity and $\log_2$ 25HC BALF concentration. Analyses were conducted using GraphPad Prism statistical software or R version 3.5.1. For all tests, $P < 0.05$ was considered significant.

Study approval. All rodent experiments were performed in accordance with the Animal Welfare Act and the US Public Health Service Policy on Humane Care and Use of Laboratory Animals after review by the Animal Care and Use Committee of the NIEHS. For the human bronchoscopic LPS studies, approval was obtained from the Colorado Multiple IRB, and informed consent was provided according to the Declaration of Helsinki. For studies in which AMs were retrieved by BAL, normal healthy volunteers completed informed consent under approval of NIEHS IRB protocol no. 11-E-0006. For the fish oil ARDS trial, participants were enrolled at 5 North American centers (62). Informed consent was obtained before study enrollment; human subject committees at each site approved the trial, as did a Data Safety Monitoring Board appointed by the National Heart, Lung, and Blood Institute (NHLBI).

Author contributions

JHM, KMG, ST, JAN, EA, SG, JMM, MJT, WJJ, DNC, and MBF designed and conducted experiments, analyzed and interpreted the data, and contributed to writing of the manuscript. EDM, JGM, BMT, CM, RDS, and MMW analyzed and interpreted the data and contributed to writing of the manuscript. GM and JM prepared essential reagents and contributed to the writing of the manuscript.

Acknowledgments

The authors thank the NIEHS Flow Cytometry Core and Ligon Perrow for assistance with animal husbandry. This research was supported by the Intramural Research Program of the NIH (NIH), NIEHS (Z01 ES102005), and by NIH National Heart, Lung, and Blood Institute (P50 HL073996 and K23 HL144916).

Address correspondence to: Michael B. Fessler, National Institute of Environmental Health Sciences, 111 T.W. Alexander Drive, P.O. Box 12233, MD D2-01, Research Triangle Park, North Carolina 27709, USA. Phone: 984.287.4081; Email: fesslerm@niehs.nih.gov.

1. Mould KJ, et al. Cell Origin Dictates Programming of Resident versus Recruited Macrophages during Acute Lung Injury. *Am J Respir Cell Mol Biol*. 2017;57(3):294–306.
2. Janssen WJ, et al. Surfactant proteins A and D suppress alveolar macrophage phagocytosis via interaction with SIRP alpha. *Am J Respir Crit Care Med*. 2008;178(2):158–167.
3. Mohning MP, et al. Phagocytosis of microparticles by alveolar macrophages during acute lung injury requires MerTK. *Am J Physiol Lung Cell Mol Physiol*. 2018;314(1):L69–L82.
4. Huynh ML, Fadok VA, Henson PM. Phosphatidylserine-dependent ingestion of apoptotic cells promotes TGF-beta1 secretion and the resolution of inflammation. *J Clin Invest*. 2002;109(1):41–50.
5. Fadok VA, Bratton DL, Konowal A, Freed PW, Westcott JY, Henson PM. Macrophages that have ingested apoptotic cells in vitro inhibit proinflammatory cytokine production through autocrine/paracrine mechanisms involving TGF-beta, PGE2, and PAF. *J Clin Invest*. 1998;101(4):890–898.
6. A-Gonzalez N, et al. Apoptotic cells promote their own clearance and immune tolerance through activation of the nuclear receptor LXR. *Immunity*. 2009;31(2):245–258.
7. Hong C, et al. Coordinate regulation of neutrophil homeostasis by liver X receptors in mice. *J Clin Invest*. 2012;122(1):337–347.
8. Fujimori T, et al. The Axl receptor tyrosine kinase is a discriminator of macrophage function in the inflamed lung. *Mucosal Immunol*. 2015;8(5):1021–1030.
9. Roberts AW, Lee BL, Deguine J, John S, Shlomchik MJ, Barton GM. Tissue-Resident Macrophages Are Locally Programmed for Silent Clearance of Apoptotic Cells. *Immunity*. 2017;47(5):913–927.e6.
10. Hu B, et al. Resident murine alveolar and peritoneal macrophages differ in adhesion of apoptotic thymocytes. *Am J Respir Cell Mol Biol*. 2004;30(5):687–693.
11. Curtis JL, Todt JC, Hu B, Osterholzer JJ, Freeman CM. Tyro3 receptor tyrosine kinases in the heterogeneity of apoptotic cell uptake. *Front Biosci (Landmark Ed)*. 2009;14:2631–2646.
12. Korns D, Frasch SC, Fernandez-Boyanapalli R, Henson PM, Bratton DL. Modulation of macrophage efferocytosis in inflammation. *Front Immunol*. 2011;2:57.
13. Fessler MB. The challenges and promise of targeting the Liver X Receptors for treatment of inflammatory disease. *Pharmacol Ther*. 2018;181:1–12.
14. Chen W, Chen G, Head DL, Mangelsdorf DJ, Russell DW. Enzymatic reduction of oxysterols impairs LXR signaling in cultured cells and the livers of mice. *Cell Metab*. 2007;5(1):73–79.
15. Diczfalusy U. On the formation and possible biological role of 25-hydroxycholesterol. *Biochimie*. 2013;95(3):455–460.
16. Bauman DR, Bitmansour AD, McDonald JG, Thompson BM, Liang G, Russell DW. 25-Hydroxycholesterol secreted by macrophages in response to Toll-like receptor activation suppresses immunoglobulin A production. *Proc Natl Acad Sci USA*. 2009;106(39):16764–16769.
17. Park K, Scott AL. Cholesterol 25-hydroxylase production by dendritic cells and macrophages is regulated by type I interferons. *J Leukoc Biol*. 2010;88(6):1081–1087.
18. Diczfalusy U, et al. Marked upregulation of cholesterol 25-hydroxylase expression by lipopolysaccharide. *J Lipid Res*. 2009;50(11):2258–2264.
19. Maurya MR, et al. Analysis of inflammatory and lipid metabolic networks across RAW264.7 and thioglycolate-elicited macrophages. *J Lipid Res*. 2013;54(9):2525–2542.
20. Reboldi A, Dang EV, McDonald JG, Liang G, Russell DW, Cyster JG. Inflammation. 25-Hydroxycholesterol suppresses interleukin-1-driven inflammation downstream of type I interferon. *Science*. 2014;345(6197):679–684.
21. Kimura T, et al. Polarization of M2 macrophages requires Lamtor1 that integrates cytokine and amino-acid signals. *Nat Commun*. 2016;7:13130.
22. Gold ES, et al. 25-Hydroxycholesterol acts as an amplifier of inflammatory signaling. *Proc Natl Acad Sci USA*. 2014;111(29):10666–10671.
23. Lund EG, Kerr TA, Sakai J, Li WP, Russell DW. cDNA cloning of mouse and human cholesterol 25-hydroxylases, polytopic membrane proteins that synthesize a potent oxysterol regulator of lipid metabolism. *J Biol Chem*. 1998;273(51):34316–34327.
24. Heng TS, Painter MW, Immunological Genome Project Consortium. The Immunological Genome Project: networks of gene expression in immune cells. *Nat Immunol*. 2008;9(10):1091–1094.
25. Smoak K, et al. Effects of liver X receptor agonist treatment on pulmonary inflammation and host defense. *J Immunol*. 2008;180(5):3305–3312.
26. Cyster JG, Dang EV, Reboldi A, Yi T. 25-Hydroxycholesterols in innate and adaptive immunity. *Nat Rev Immunol*. 2014;14(11):731–743.
27. Lai L, et al. MicroRNA-33 Regulates the Innate Immune Response via ATP Binding Cassette Transporter-mediated Remodeling of Membrane Microdomains. *J Biol Chem*. 2016;291(37):19651–19660.
28. Gautier EL, et al. Systemic analysis of PPARγ in mouse macrophage populations reveals marked diversity in expression with critical roles in resolution of inflammation and airway immunity. *J Immunol*. 2012;189(5):2614–2624.
29. Mei J, et al. CXCL5 regulates chemokine scavenging and pulmonary host defense to bacterial infection. *Immunity*. 2010;33(1):106–117.
30. Castrillo A, et al. Crosstalk between LXR and toll-like receptor signaling mediates bacterial and viral antagonism of cholesterol metabolism. *Mol Cell*. 2003;12(4):805–816.
31. Draper DW, Madenspacher JH, Dixon D, King DH, Remaley AT, Fessler MB. ATP-binding cassette transporter G1 deficiency

dysregulates host defense in the lung. *Am J Respir Crit Care Med*. 2010;182(3):404–412.
32. Bates SR, Tao JQ, Collins HL, Francone OL, Rothblat GH. Pulmonary abnormalities due to ABCA1 deficiency in mice. *Am J Physiol Lung Cell Mol Physiol*. 2005;289(6):L980–L989.
33. Scott RS, et al. Phagocytosis and clearance of apoptotic cells is mediated by MER. *Nature*. 2001;411(6834):207–211.
34. Fond AM, Lee CS, Schulman IG, Kiss RS, Ravichandran KS. Apoptotic cells trigger a membrane-initiated pathway to increase ABCA1. *J Clin Invest*. 2015;125(7):2748–2758.
35. Kiss RS, Elliott MR, Ma Z, Marcel YL, Ravichandran KS. Apoptotic cells induce a phosphatidylserine-dependent homeostatic response from phagocytes. *Curr Biol*. 2006;16(22):2252–2258.
36. Borges VM, et al. TNFalpha inhibits apoptotic cell clearance in the lung, exacerbating acute inflammation. *Am J Physiol Lung Cell Mol Physiol*. 2009;297(4):L586–L595.
37. Miyanishi M, Tada K, Koike M, Uchiyama Y, Kitamura T, Nagata S. Identification of Tim4 as a phosphatidylserine receptor. *Nature*. 2007;450(7168):435–439.
38. Uderhardt S, et al. 12/15-lipoxygenase orchestrates the clearance of apoptotic cells and maintains immunologic tolerance. *Immunity*. 2012;36(5):834–846.
39. Wong K, Valdez PA, Tan C, Yeh S, Hongo JA, Ouyang W. Phosphatidylserine receptor Tim-4 is essential for the maintenance of the homeostatic state of resident peritoneal macrophages. *Proc Natl Acad Sci USA*. 2010;107(19):8712–8717.
40. Li Z, et al. Krüppel-Like Factor 4 Regulation of Cholesterol-25-Hydroxylase and Liver X Receptor Mitigates Atherosclerosis Susceptibility. *Circulation*. 2017;136(14):1315–1330.
41. Mass E, et al. Specification of tissue-resident macrophages during organogenesis. *Science*. 2016;353(6304):aaf4238.
42. Baldan A, et al. ABCG1 is required for pulmonary B-1 B cell and natural antibody homeostasis. *J Immunol*. 2014;193(11):5637–5648.
43. Sekiya M, et al. Absence of Nceh1 augments 25-hydroxycholesterol-induced ER stress and apoptosis in macrophages. *J Lipid Res*. 2014;55(10):2082–2092.
44. Gautier EL, et al. Gene-expression profiles and transcriptional regulatory pathways that underlie the identity and diversity of mouse tissue macrophages. *Nat Immunol*. 2012;13(11):1118–1128.
45. Sugiura H, et al. Increased 25-hydroxycholesterol concentrations in the lungs of patients with chronic obstructive pulmonary disease. *Respirology*. 2012;17(3):533–540.
46. Spann NJ, et al. Regulated accumulation of desmosterol integrates macrophage lipid metabolism and inflammatory responses. *Cell*. 2012;151(1):138–152.
47. Gold ES, et al. ATF3 protects against atherosclerosis by suppressing 25-hydroxycholesterol-induced lipid body formation. *J Exp Med*. 2012;209(4):807–817.
48. Zagórska A, Través PG, Lew ED, Dransfield I, Lemke G. Diversification of TAM receptor tyrosine kinase function. *Nat Immunol*. 2014;15(10):920–928.
49. Choi JY, Seo JY, Yoon YS, Lee YJ, Kim HS, Kang JL. Mer signaling increases the abundance of the transcription factor LXR to promote the resolution of acute sterile inflammation. *Sci Signal*. 2015;8(365):ra21.
50. Camenisch TD, Koller BH, Earp HS, Matsushima GK. A novel receptor tyrosine kinase, Mer, inhibits TNF-alpha production and lipopolysaccharide-induced endotoxic shock. *J Immunol*. 1999;162(6):3498–3503.
51. Rothlin CV, Ghosh S, Zuniga EI, Oldstone MB, Lemke G. TAM receptors are pleiotropic inhibitors of the innate immune response. *Cell*. 2007;131(6):1124–1136.
52. Jennings JH, Linderman DJ, Hu B, Sonstein J, Curtis JL. Monocytes recruited to the lungs of mice during immune inflammation ingest apoptotic cells poorly. *Am J Respir Cell Mol Biol*. 2005;32(2):108–117.
53. Lee YJ, et al. Inhibiting Mer receptor tyrosine kinase suppresses STAT1, SOCS1/3, and NF-κB activation and enhances inflammatory responses in lipopolysaccharide-induced acute lung injury. *J Leukoc Biol*. 2012;91(6):921–932.
54. Liu Y, et al. 25-Hydroxycholesterol activates the expression of cholesterol 25-hydroxylase in an LXR-dependent mechanism. *J Lipid Res*. 2018;59(3):439–451.
55. Girão H, Pereira P, Ramalho J, Quinlan R, Prescott A. Cholesterol oxides mediated changes in cytoskeletal organisation involves Rho GTPases. *Exp Cell Res*. 2003;291(2):502–513.
56. Frasch SC, et al. Signaling via macrophage G2A enhances efferocytosis of dying neutrophils by augmentation of Rac activity. *J Biol Chem*. 2011;286(14):12108–12122.
57. Liu C, et al. Oxysterols direct B-cell migration through EBI2. *Nature*. 2011;475(7357):519–523.
58. Raccosta L, et al. The oxysterol-CXCR2 axis plays a key role in the recruitment of tumor-promoting neutrophils. *J Exp Med*. 2013;210(9):1711–1728.
59. Bielska AA, et al. Side-chain oxysterols modulate cholesterol accessibility through membrane remodeling. *Biochemistry*. 2014;53(18):3042–3051.
60. Cohen PL, et al. Delayed apoptotic cell clearance and lupus-like autoimmunity in mice lacking the c-mer membrane tyrosine kinase. *J Exp Med*. 2002;196(1):135–140.
61. Nick JA, et al. Recombinant human activated protein C reduces human endotoxin-induced pulmonary inflammation via inhibition of neutrophil chemotaxis. *Blood*. 2004;104(13):3878–3885.
62. Stapleton RD, et al. A phase II randomized placebo-controlled trial of omega-3 fatty acids for the treatment of acute lung injury. *Crit Care Med*. 2011;39(7):1655–1662.
63. Morrell ED, et al. Peripheral and Alveolar Cell Transcriptional Programs Are Distinct in Acute Respiratory Distress Syndrome. *Am J Respir Crit Care Med*. 2018;197(4):528–532.
64. Du P, Kibbe WA, Lin SM. lumi: a pipeline for processing Illumina microarray. *Bioinformatics*. 2008;24(13):1547–1548.
65. McDonald JG, Thompson BM, McCrum EC, Russell DW. Extraction and analysis of sterols in biological matrices by high performance liquid chromatography electrospray ionization mass spectrometry. *Meth Enzymol*. 2007;432:145–170.
66. Martinez J, et al. Microtubule-associated protein 1 light chain 3 alpha (LC3)-associated phagocytosis is required for the efficient clearance of dead cells. *Proc Natl Acad Sci USA*. 2011;108(42):17396–17401.
67. Draper DW, et al. ATP binding cassette transporter G1 deletion induces IL-17-dependent dysregulation of pulmonary adaptive immunity. *J Immunol*. 2012;188(11):5327–5336.